Thermally induced errors in diamond turning of optical structured surfaces

Stefan Rakuff
2 Barclay Street
Clifton Park, New York 12065
E-mail: rakuff@gmail.com

Paul Beaudet*
Paul Beaudet & Associates, Inc.
4604 Greenbriar Court
Boulder, Colorado 80303

Abstract. Thermally induced errors were identified as a large error source during diamond turning of micrometer-size optical structures. We investigate the effects of spindle growth, application of cutting fluid mist, and temperature variation errors (TVEs), or thermal drifts, on the ability to hold tool position tolerances. It is shown how certain process variables, such as opening and closing of doors around the machine, affect the TVE. A first-order temperature model was derived to predict the TVE of the manufacturing process. The model uses the ambient temperature inside the machine enclosure because the part temperature could not be measured directly during machining. Documented long-term drift errors over 23 h were as large as 1.7 μm. Short-term drift errors from pass to pass were as large as 0.3 μm. Transient effects caused displacement shifts as large as 0.9 μm. © *2007 Society of Photo-Optical Instrumentation Engineers.* [DOI: 10.1117/1.2795571]

Subject terms: optical structured surfaces; diamond turning; temperature variation errors (TVE); thermal drift.

Paper 070043R received Jan. 16, 2007; revised manuscript received May 8, 2007; accepted for publication May 11, 2007; published online Oct. 24, 2007.

1 Introduction

Optically structured surfaces are surfaces that contain deterministic patterns of usually high aspect ratio geometric features designed to give a specific function.[1] Examples of structured surfaces include the reflective coatings on road signs, self-cleaning surfaces, drag reduction films, and diffraction gratings. The size of the structures on the surface is commonly orders of magnitude smaller than the overall size of the part itself, requiring high precision during fabrication. This paper deals with master cylinders that have structured surfaces machined on the outer diameter. These cylinders have applications in, for example, roll-to-roll manufacturing of organic electronic components, such as organic light emitting diodes (OLED), or the manufacture of engineered optical films for liquid crystal displays (LCDs).[2] The cylinders discussed in this study were 7.0 in. long and 5.0 in. in outer diameter. The cylinder consisted of a 6061 T6 aluminum substrate with a wall thickness of 1.0 in., shown in Fig. 1. The outer surface of the substrate was plated with udylite bright acid copper (UBAC), with plating thicknesses between 0.05 in. and 0.06 in.

A T-base diamond turning machine (DTM) with 200 mm $\times$ 200 mm axis travel was used for the necessary precision fabrication steps that generate the structured surfaces. In a typical machining operation, an optical mirror finish was machined onto the outer diameter and free end face of the cylinder. This removed eccentricity, out-of-roundness, tilt, and total indicator run out in the axial and radial directions. Prismatic structures were then machined on the outer diameter of the cylinder, as shown in the cross section in Fig. 1. The prisms formed a thread with a pitch of 37 μm per revolution. The radius at the valleys and peaks of the prisms was 5 μm. The microstructures had to be machined in multiple passes and using multiple diamond cutting tools. The required repositioning tolerances for the diamond cutting tool are very small compared to the overall part size, and thermally introduced errors became significant.

2 Error Sources in the Fabrication Process

Dark-field microscopy images, such as Fig. 2, were used for on-machine visual inspection of the microstructures. The valleys and peaks are visible as dark and bright vertical lines, respectively. Defects were seen in the form of chatter on the prism flanks, burring along the center of the valleys, and double valleys. The double valleys could have been caused by tool tip damage or axial non-repeatability of the tool position during consecutive passes. Nickel electroforms were utilized to replicate the surface structure of the cylinders. The electroform replicas were inspected using a scanning electron microscope (SEM).

Figure 3 shows an SEM image. The peak near the center of the image corresponded to a valley of the pattern on the

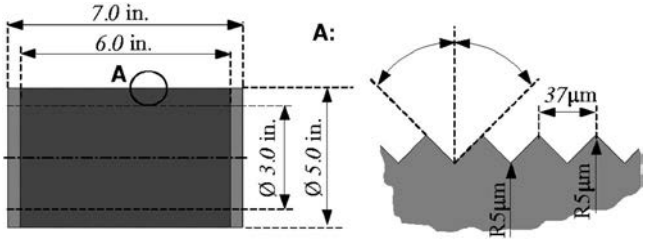

Fig. 1 Sketch of side view of microstructured cylinder.

*Tel: 303–908–8351; E-mail: sneaudet@yahoo.com

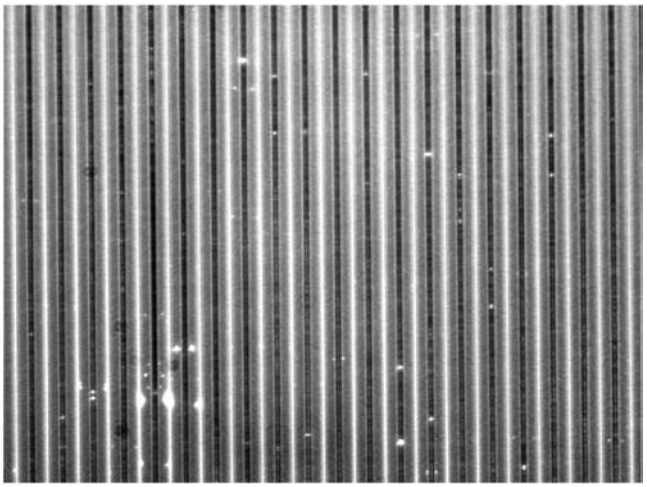

Fig. 2 Microscopic image of microstructures cut on the cylinder. The pitch of the structure was 37 μm. Valleys (dark vertical lines) appeared as double valleys that were potentially caused by tool misalignments.

actual cylinder. A defect band of approximately 0.3 μm in width was visible near the ridge. A vertical line was visible that separated regions of small and large chatter. The large chatter was likely created during the 7-μm pass, whereas the small chatter was likely left behind during the finish pass. Both defects were potentially caused by nonrepeatability of the tool position.

The discussed defects could be attributed to thermal, geometric, or elastic errors. These error sources affect the structural loop of the machine, as indicated in Fig. 4. Geometric errors are the result of linear and angular error motions inherent to the machine. Elastic errors are static or dynamic deformations of the machine. They can be caused, for example, by gravity sag, clamping forces, or inertia effects and vibrations. Temperature errors can be caused by external heat sources, such as direct sunlight, or internal heat sources, such as electric motors and amplifiers. Thermal error sources investigated here included spindle growth, errors due to misting of cutting fluids, and temperature variation errors (TVEs) or thermal drifts. TVEs were found to be sensitive to the opening and closing of machine enclosure doors and laboratory doors and the cycling time of the room air temperature controller.

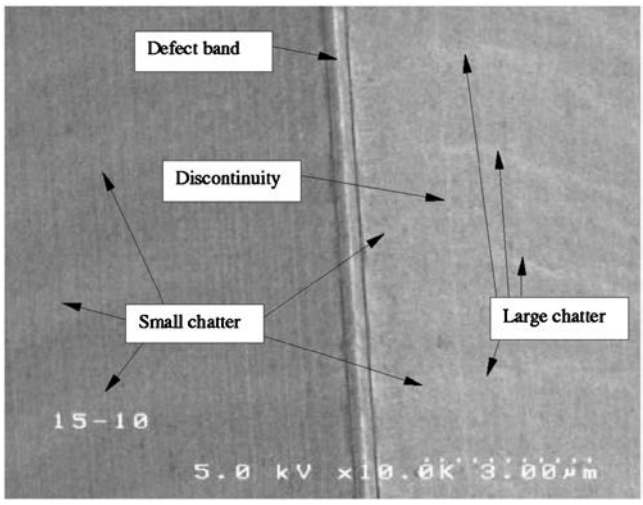

Fig. 3 SEM photograph of a nickel electroform containing a defect near the center ridge. Also visible were regions of large and small chatter separated by a distinct line.

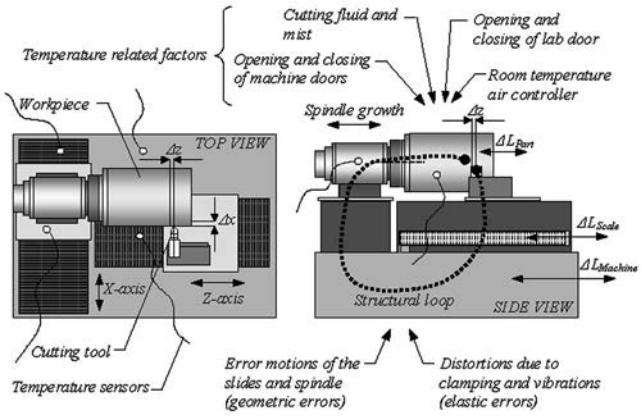

Fig. 4 Thermal, geometric, and elastic error sources affecting the structural loop of the cylinder diamond turning process, creating an axial tool offset.

The error was defined as the offset of the cutting tool with respect to the cylinder at the free end. The error had an axial component Δz and a radial component Δx and is the sum of the expansions of the cylinder ΔL_{Part}, the granite machine base $\Delta L_{\text{Machine}}$, and the glass scale for position control ΔL_{Scale}. Given a temperature rise and expanding components, ΔL_{Part} is positive and $\Delta L_{\text{Machine}}$ and ΔL_{Scale} are negative, assuming that the scale is attached to the base on the left and allowed to expand on the right (Fig. 4).

3 Thermal Tests

3.1 *Description of Test Setup*

Many researchers have derived temperature models of machine tools and were able to predict thermally induced errors based on the temperature distribution within the machine. Temperature sensors were often attached to the machines that were then used for various thermal compensation techniques.[3–5] In this study, most of the TVE is caused by part drifts ΔL_{Part} rather than $\Delta L_{\text{Machine}}$ or ΔL_{Scale}. The part was exposed to higher airflows while the machine axis and scales were covered with bellows and mounted on a large granite base. The granite base had a lower coefficient of thermal expansion (CTE) and higher heat capacity than the part. The axis of rotation of the part when rotating could not be disturbed by installing temperature sensors on the part surface. Instead, ambient temperatures were recorded at spindle center height inside the machine enclosure.

Temperature and displacements Δz and Δx were measured using a Lion Precision spindle error analyzer (SEA), consisting of a three-channel capacitance probe system, temperature sensors, digital data acquisition hardware from National Instruments, and Lab View-based analysis software. The SEA can be utilized as a diagnostic instrument for long-term thermal drift tests or to measure rotational error motions of spindles that require high sampling fre-

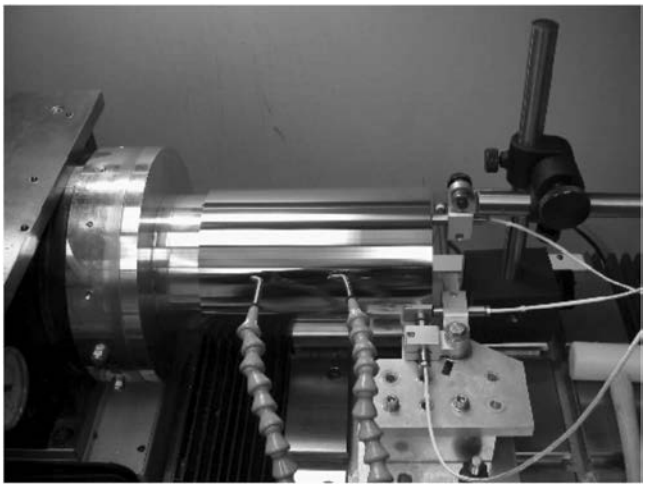

Fig. 5 Axial and radial capacitance probes mounted on the tool post and axial capacitance probe mounted off the magnetic base on a *z*-axis table. Mister nozzles #1 (left) and #2 (right) were used to determine the effect of cutting fluid on cylinder expansion.

quencies. Figure 5 shows axial and radial capacitance probes mounted on the tool post at the free end of the cylinder, following the illustrations for the two-probe temperature test in ASME B5.57 (Ref. 6). This setup ensured that the capacitance probes measured the same relative displacements as seen by the cutting tool. Positive displacements meant that the air gap between the part and the probe shrinks, and negative displacements indicated that the air gap increases. When mounting the capacitance gauges using magnetic bases, the measurements of thermal drift were distorted due to expansion of the magnetic bases. The two mister nozzles were used to apply cutting fluid mist to simulate machining runs.

3.2 *Spindle Growth*

Heat from the spindle is generally a significant error source in machine tools.[7] The heat is generated by the spindle motor and air shear in the air bearings and affects thermal growth and distortion of the spindle housing and shaft. Spindle growth was anticipated in this study because the existing spindle is not chilled. The growth can cause deformations in all five degrees of freedom, but only the effective axial and radial relative position shifts on the free end of the cylinder were measured with the existing test setup. Thermal spindle growth is typically determined with the spindle operating at certain speeds and load patterns.[6,8] The test procedure utilized in this paper was to run the initially cold spindle at 100 rpm, a typical spindle speed during machining, and neglect loads created by the cutting tool.

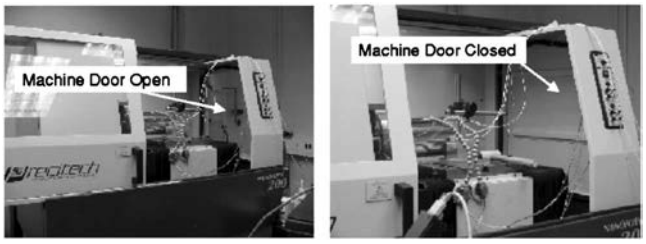

Fig. 7 Photographs of DTM showing side door open (left) and closed (right).

Initially, the magnitude of the axial and radial displacements rates were 4.0 μm/h (Fig. 6). After 4.5 h, the displacement rates were approximately 0.07 μm/h. Viewed from a tool coordinate system, the free end of the cylinder moved 3.8 μm to the left and 3.2 μm away from the tool. Axial spindle growth was considered more critical since it caused a constant offset error of the cutting tool that was independent of the *z*-axis position. The data shows that the spindle needed to warm up for 2 h to decrease the axial spindle growth rate to 0.4 μm/h.

3.3 *Effect of Machine Side Access Door on TVE*

The machine side access door, shown in Fig. 7, was sometimes open during machining operations for purposes of chip control, to gain access to the mister nozzles for cutting fluid application, and for monitoring the cutting process. A test with a stationary spindle was set up to measure the effects of opening the side door. At the beginning of the test, the side door was open, and the resulting temperature swings were 2 °C (Fig. 8). The resulting radial and axial displacement amplitudes with respect to the cutting tool location were 0.2 μm and 0.3 μm, respectively.

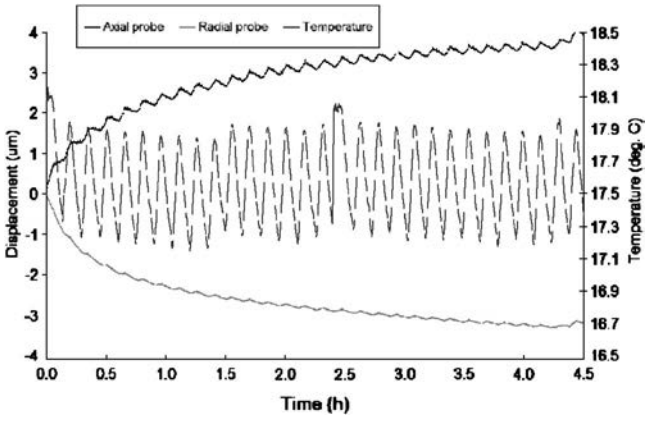

Fig. 6 Axial and radial displacements measured while the spindle was rotating at 100 rpm. Spindle was cold at startup.

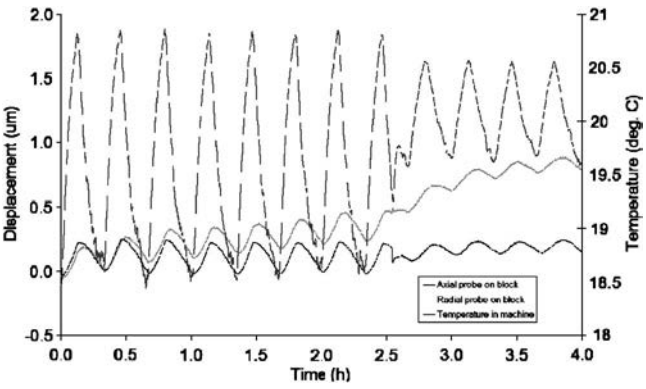

Fig. 8 Effects of open and closed machine side access door on dimensional stability in axial and radial directions as seen by the cutting tool at the free end of the cylinder.

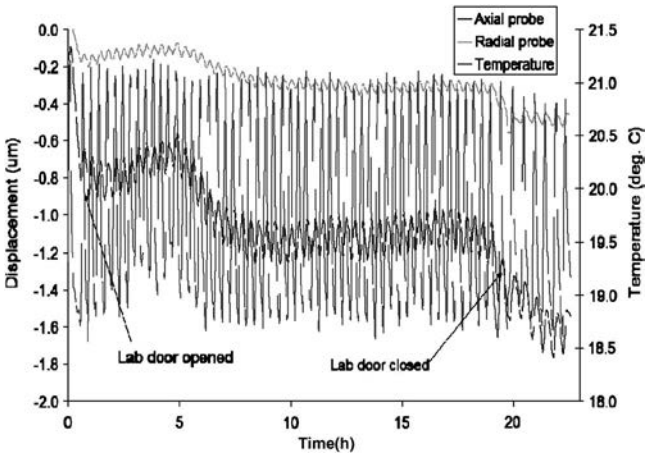

Fig. 9 Long-term drift test over a weekend for 23 h with no traffic in the laboratory.

When the machine side door was closed 2.5 h into the test, the total temperature swing inside the machine dropped to 1 °C. The radial and axial displacement swings were reduced to 0.1 μm. The mean temperature increased by 0.5 °C with the side door closed. The resulting shifts of the average axial and radial displacements were 0.1 μm and 0.4 μm, respectively. The temperature increase inside the machine was partly caused by internal heat sources such as the linear axis motors and the oil pump.

3.4 *Long-Term TVE Test with Laboratory Door Closed and Open*

A long-term TVE test was conducted over a weekend with no traffic in the laboratory. Two capacitance gauges were mounted off the z-axis table to monitor axial and radial displacements of the free end of the cylinder with respect to the z-axis table. Figure 9 shows temperature and displacement data recorded over 23 h with the machine door open. During the first hour, temperature transients were visible that could have been caused by people in the laboratory. The average radial and axial displacement shifted by 0.2 μm and 0.8 μm, respectively. This was likely caused by ambient temperature transients and temperature gradients of the magnetic bases. Long-term changes of the average temperature between hours 1 and 19 caused average axial and radial displacements of 0.4 μm and 0.1 μm.

Figure 10 shows the last 8 h of the test. The temperature cycled with a period of 20 min before the laboratory door was closed toward the end of the test. The corresponding peak-to-valley displacement was 0.20 μm axially and 0.05 μm radially. When the door was closed, the temperature cycling time increased to 30 min, causing axial and radial peak-to-valley displacements of 0.25 μm and 0.05 μm, respectively. The increase of the period can be explained by noting that warmer air from the outside room was prevented from flowing into the laboratory with the door shut. This caused the temperature controller to cycle less frequently. Transient effects were seen when the laboratory door was closed, causing 0.6-μm and 0.2-μm shifts in the axial and radial directions, respectively.

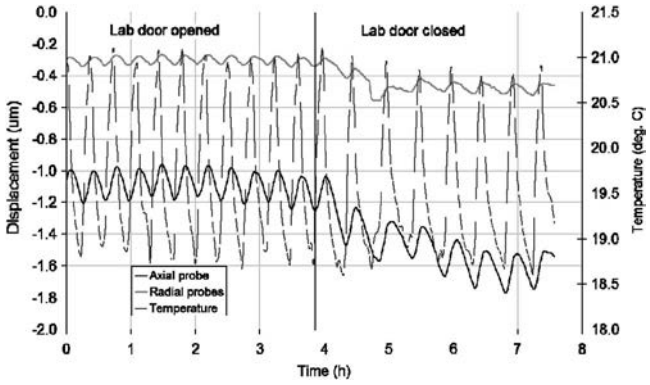

Fig. 10 The temperature cycle increases from 20 to 30 min when the laboratory door is closed, resulting in larger axial and radial displacements.

4 Effects of Applying Cutting Fluid

4.1 *Misting of Cutting Fluid*

Odorless mineral spirits (OMS) was used as cutting fluid during machining. One of the purposes of cutting fluid was the prevention of a built-up edge on the rake face of the cutting tool. Temperature-controlled oil mists also have been used in the past to thermally stabilize machines and workpieces.[9,10] It was suspected that the mist of cutting fluid could affect the thermal sensitivity of cylinders in the machine. A test was performed to investigate the effects of OMS sprayed onto the cylinder as a cutting fluid during simulated machining runs. The machine side access door was left open during the tests, and the spindle was thermally stable at 100 rpm. In the first 6 h, the peak-to-valley axial and radial TVEs were 0.2 μm and 0.3 μm, respectively (Fig. 11).

The two mister nozzles positioned along the cylinder (Fig. 5) were turned on and off after one another to simulate 30-min cutting passes. The mist was started after 1.3 h by turning on mister nozzle #1 for 15 min. This generated a 2-in.-wide band of OMS on the part. Immediately thereafter, mister nozzle #2 was turned on for 15 min more, cre-

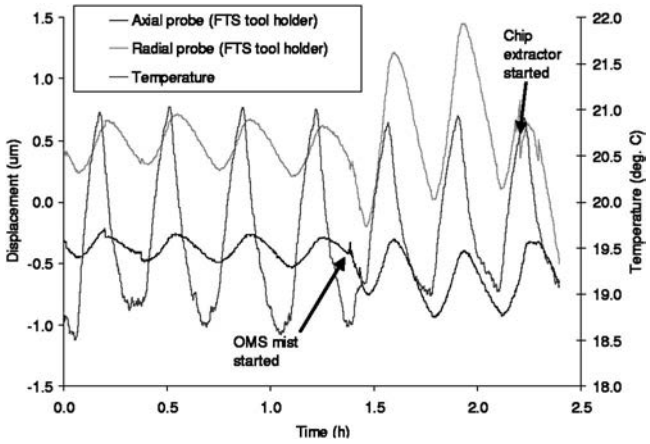

Fig. 11 Axial and radial displacement variations while the part is rotated at 100 rpm. After 1.3 h, the OMS mister nozzles were activated one at a time for 15 min to simulate 30-min passes. A chip extractor was installed and operated after 2.2 h.

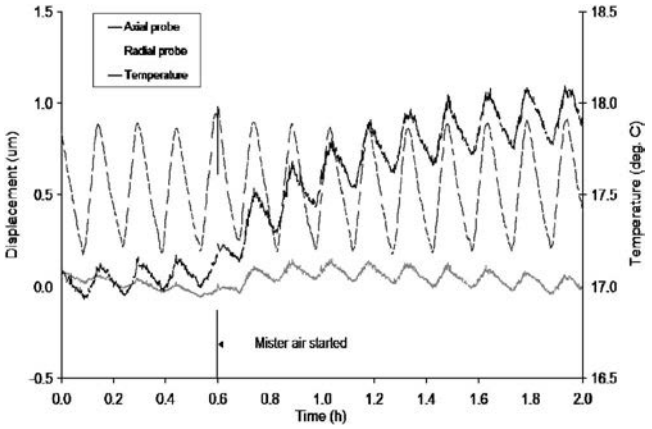

Fig. 12 Air blowing through the mister nozzles was started 0.6 h into the test, causing larger peak-to-valley displacements as well as axial and radial shifts.

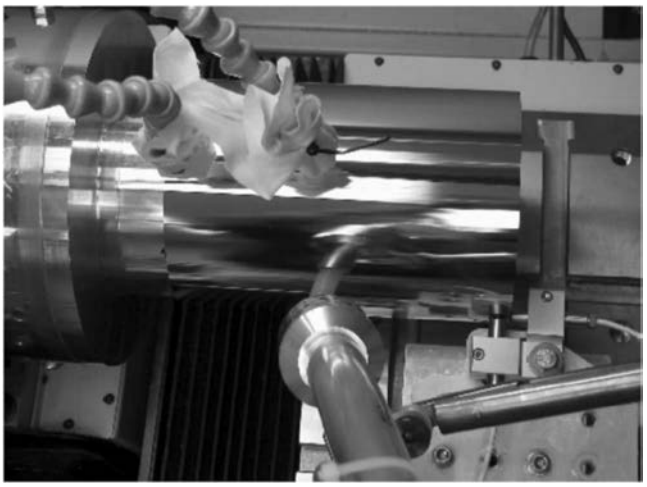

Fig. 13 Mister nozzles were blocked off to allow dripping of the cutting fluid. Axial and radial capacitance probes were mounted on the tool post, and a chip extractor was installed above the tool position.

ating another 2-in.-wide band of OMS while the first band of OMS evaporated. Four consecutive passes were simulated this way. The data in Fig. 11 shows that the peak-to-valley values of axial and radial TVEs increased to 0.9 μm and 0.5 μm, respectively. Misting OMS amplified the effect of room temperature swings on the part. A chip extractor was installed after 2.2 h with no measurable effect. The radial probe was bumped when setting up.

4.2 *Air Only from Mister Nozzles*

A test was performed with only air flowing out of the mister nozzles. The machine side door was closed, leading to short-term temperature variations of only 0.7 °C (Fig. 12). Before the air was turned on, the peak-to-valley axial and radial displacements were 0.2 μm and 0.05 μm. With air from the misters turned on, after 0.6 h, the peak-to-valley axial and radial displacements increased to 0.5 μm and 0.1 μm. Over the next 1.6 h, the average axial and radial positions shifted by 0.9 μm and 0.1 μm, respectively. The data also show that the airflow did not change the ambient temperature inside the machine.

4.3 *Dripping of Cutting Fluid*

The mister nozzles were blocked off, as shown in Fig. 13, before beginning the test. This allowed dripping of OMS onto the spinning part. The average axial and radial displacement shifts caused by spindle deformations and growth were 0.8 μm and −0.5 μm over 3.5 h (Fig. 14). After 3.8 h, OMS cutting fluid was dripped onto the part, causing the mean radial and axial positions to shift by 0.4 μm and 0.5 μm, respectively. The drops formed a film of OMS on only the left portion of the part to avoid contamination of the capacitance probes. The axial and radial short-term variations did not change in magnitude with dripping of cutting fluid.

5 Analysis of Temperature Test Data

A thermal model was established to relate the TVE of the cutting tool to changes in the ambient temperature in the machine enclosure. The model made it possible to make TVE predictions during machining with a temperature sensor installed inside the machine enclosure without the need to install temperature sensors on the cylinder. As described earlier, the total TVE is the sum of scale, machine, and cylinder drifts. Machine and scale drifts were negligible compared to cylinder drifts because the machine represented a large thermal mass, and the scales were made of low-expansion glass and enclosed in bellows. Hence, instead of making corrections for differential expansions, all machine and scale drifts were lumped into the thermal model for the cylinder. The temperature distribution inside the cylinder was assumed to be nearly uniform because of the good thermal conductivity of aluminum. Therefore, the length change of the cylinder ΔL_D at a given cylinder temperature T_D was calculated using:

$$\Delta L_D = \alpha_{AL} L_{D,20} (T_D - 20\,^\circ\mathrm{C}). \quad (1)$$

The linear CTE of 6061 T6 aluminum α_{AL} equals 23.8 $\times 10^{-6}/\,^\circ$C. The uncertainty in the CTE was assumed to be 20 percent.[11] $L_{D,20}$ was 17.80 cm, the length of the cylinder at 20 °C. Length variations of the cylinder can be deter-

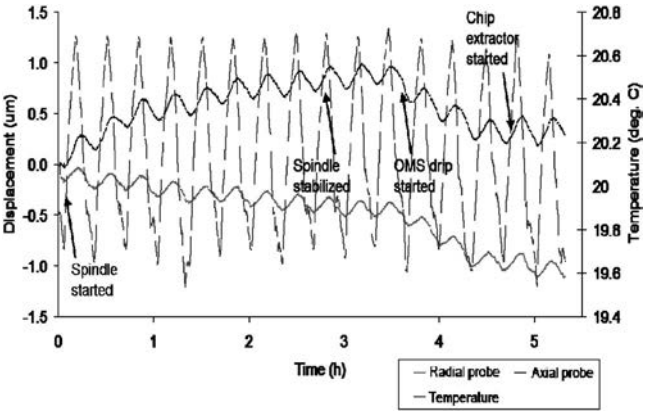

Fig. 14 Cutting fluid dripped on the part starting after 3.8 h, causing position shifts but no change in peak-to-valley displacements. Spindle deformations and growth resulted in axial and radial drifts.

mined if the cylinder temperature T_D is known at all times. Since T_D cannot be measured directly, a temperature sensor was installed in the machine enclosure to measure the ambient temperature T_A. Bernoulli's equation was used to relate T_A to the cylinder temperature T_D:

$$m_D c_P \frac{dT_D}{dt} = hA_D(T_A - T_D). \tag{2}$$

Here, m_D is the mass of the part, c_P the specific heat of aluminum, A_D the effective surface area of the part, and h the overall heat transfer coefficient. Equation (2) can be brought in the form:

$$\frac{dT_D}{dt} + \gamma T_D = \gamma T_A, \tag{3}$$

where

$$\gamma = \frac{hA_D}{m_D c_P}. \tag{4}$$

The ambient temperature swings were modeled using a sinusoidal function with amplitude T_0 and constant bias temperature T_B of 20 °C:

$$T_A = T_B + T_0 \sin \omega t. \tag{5}$$

This temperature model is simple enough that a closed-form solution of Eq. (2) can be found by integration. Substitution of Eqs. (4) and (5) into Eq. (3) yields the solution:

$$T_D = T_B + \frac{\gamma T_0}{(\gamma^2 + \omega^2)^{1/2}} \sin(\omega t - \delta) + ce^{-\gamma t}, \tag{6}$$

with

$$\delta = \arctan \frac{\omega}{\gamma}. \tag{7}$$

The frequency ω and amplitude T_B for the temperature model were obtained by fitting Eq. (5) to actual temperature data, and the constant γ was determined by fitting Eqs. (6) and (1) to the axial displacement data. Fits were performed for three displacement measurements, yielding:

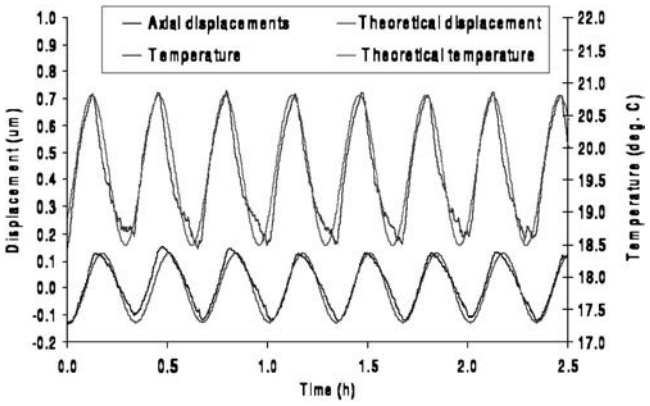

Fig. 15 Fit to ambient temperature (top) and axial displacement data (bottom).

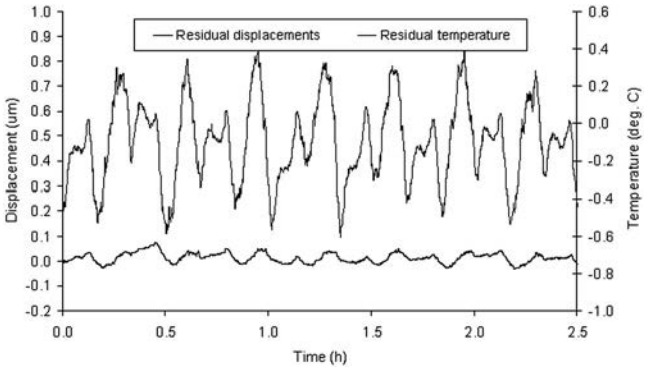

Fig. 16 Residuals of fits to temperature and axial displacement. The residuals did not follow a normal distribution, but the amplitude errors of axial displacement fit did not exceed 25 nm, ignoring phase shifts.

$$\gamma = (133 \pm 8) \cdot 10^{-6}/\text{s}. \tag{8}$$

An example of fitting temperature and displacement data is shown in Fig. 15. The residuals of the fits are shown in Fig. 16. The residuals did not follow a normal distribution because higher-order regression terms were neglected in forcing function (5). However, when neglecting phase shift errors of the fit, the predicted magnitudes of TVE fell within 25 nm of the measured values.

The constant γ increased when curve fitting to data that was obtained when the OMS mister was running:

$$\gamma_M = 594 \cdot 10^{-6}/\text{s}. \tag{9}$$

The increase of γ indicated that the part became more sensitive to temperature excursions. The constant c in Eq. (6) depends on the initial temperature conditions. Ignoring transients, c was set to zero, and Eqs. (6) and (1) were used to predict TVEs of the part for given temperature measurements.

Figures 17 and 18 show the predicted TVEs for various temperature amplitudes inside the machine without and with the mister.

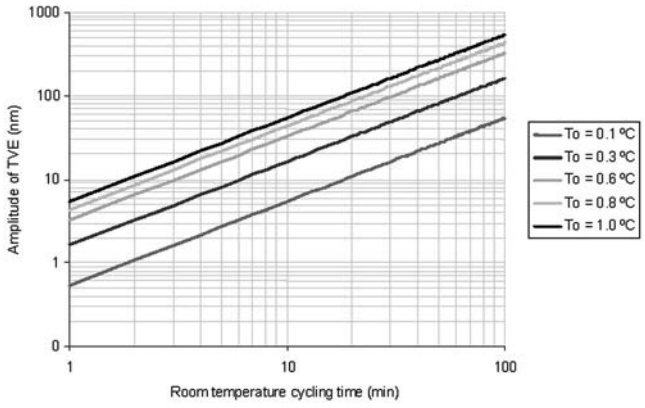

Fig. 17 Predicted TVEs of the part for different temperature amplitudes inside the machine.

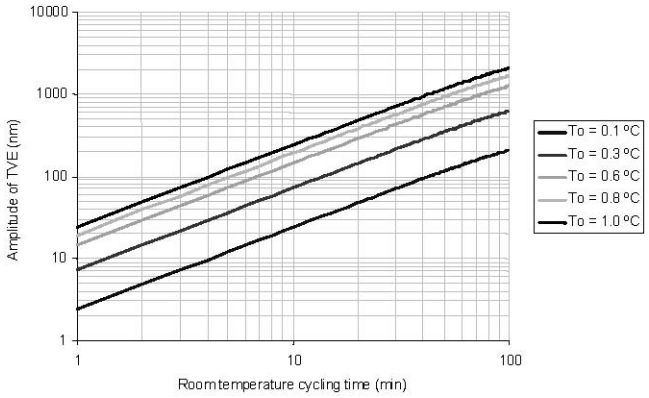

Fig. 18 Predicted TVEs of the part for different temperature amplitudes inside the machine with the OMS mister in use.

6 Summary of Results and Discussion

The data show that oscillatory steady-state positioning errors were driven by short-term temperature variations and transient positioning errors were due to a special cause such as spindle growth or opening or closing of the laboratory door. Table 1 summarizes the transient errors and their cause. It is seen that spindle growth produced axial and radial errors that were orders of magnitude larger than other errors. Table 2 summarizes the peak-to-valley errors that resulted from certain operating conditions. The largest errors were seen with the application of mist or air.

To reduce temperature-induced errors in the cylinder fabrication process, the following procedures are recommended:

- Spindle growth should be minimized to 0.4 μm/h by starting the spindle approximately 2 h before machining begins.
- The part and tooling should be allowed to stabilize on the machine for several hours or over night before machining begins.
- The laboratory door should remain either open or closed starting 2 h before and during machining. Preferably, the door should remain open, causing high-frequency temperature variations. High-frequency variations are preferred over low-frequency variations because of the large thermal time constants associated with the machine.
- Critical tool stack components should be handled with insulated gloves.
- Cutting fluid should be applied before machining begins until the part stabilizes.
- For thermal stability, the cutting fluid should be dripped onto the part. Dripping causes less process dimensional variation than misting.
- The side door on the machine should remain closed at all times for short-term and long-term dimensional stability.
- Temperature probes should be used during machining to monitor temperature variations, and the thermal model derived in this study should be used to estimate theoretical TVE. The depth of cut should not exceed the variation that occurred between two consecutive passes.

Table 1 Summary of test results showing the transient axial and radial displacement shift due to special cause variation.

Special cause action	Radial shift (μm)	Axial shift (μm)	Time (h)
Internal heat generation in the spindle at 100 rpm	−3.2	3.8	4.5
Closing the machine side door	0.4	0.1	1.0
Handling and setting up capacitance gauges	−0.2	−0.8	1.0
Long-term temperature fluctuations	0.1	0.4	18
Changing the laboratory door	−0.2	−0.6	2.0
Starting air on mister nozzle	0.1	0.9	1.0

Table 2 Summary of test results showing the peak-to-valley short-term axial and radial displacement shifts for various machine operating conditions.

		PV radial (μm)	PV axial (μm)
Machine door	Open	0.2	0.3
	Closed	0.1	0.1
Laboratory door	Open	0.05	0.20
	Closed	0.05	0.25
OMS mist	No spray mist	0.2	0.3
	Spray mist on	0.5	0.9
Mist air only	Air off	0.2	0.05
	Air enabled	0.5	0.1
OMS droplets	No OMS	0.2	0.2
	OMS dripping	0.2	0.3

Continuous testing and documentation of ambient temperature is recommended even after a few good cylinders have been machined. To prevent degradation of the process and scrap cylinders, temperature measurements should be analyzed continuously to take corrective actions as described earlier.

7 Conclusions

A first-order temperature model was derived from experimental results that allowed estimation of TVE without mea-

suring the cylinder temperature directly. The sensitivity of the model increases with the misting of OMS cutting fluid. A variety of variables were identified that affect the magnitude of temperature-induced error motions of the cutting tool with respect to the part. Oscillatory steady-state errors could be minimized by closing the machine door and dripping the coolant. Transients could be minimized by good operator practice to avoid disturbing the ambient temperature. Spindle growth was shown to be a big potential error source that can be minimized by running the spindle prior to machining. Consideration must be given to the temperature effects on probe holders during thermal testing.

Acknowledgments

The authors would like to thank Drs. F. Azad and D. Coyle as well as S. Hayashi and P. Myers for their valuable contributions to this study.

References

1. C. J. Evans and J. B. Bryan, *Ann. CIRP.* **48**(2), 541–556 (1999).
2. E. G. Olczak, M. Yamada, D. J. Coyle, and D. R. Olson, *SID International Symposium Digest of Technical Papers*, 1336 (2006).
3. Y. Hatamura, T. Nagao, M. Mitsuishi, M. S. Kato, S. Taguchi, T. Okumura, G. Nakagawa, and H. Sugishita, *Ann. CIRP* **42**(1), 549–552 (1993).
4. N. Srinivasa and J. C. Ziegert, *Precis. Eng.* **19**, 112–132 (1996).
5. F. L. M. Delbressine, G. H. J. Florussen, L. A. Schijvenaars, and P. H. J. Schellekens, *Precis. Eng.* **30**(1), 47–53 (2006).
6. ASME B5.57 (1998).
7. J. B. Bryan, *Ann. CIRP* **39**(2), 645–657 (1990).
8. ISO 230-3, Part 3, ISO, Geneva, Switzerland (2001).
9. J. B. Bryan, D. L. Carter, R. W. Clouser, and J. H. Hamilton, *SME Technical Paper Series IQ*, 17 (1982).
10. D. B. Debra, R. A. Victor, and J. B. Bryan, *Ann. CIRP* **35**(1), 359–363 (1986).
11. J. B. Bryan, Chapter 8, in *Coordinate Measuring Machines and Systems*, 1st ed., J. A. Bosch, Ed., pp. 227–264, Marcel Dekker, New York (1995).

Stefan Rakuff joined General Electric (GE) Global Research in January 2005. His responsibilities include development of micromachining expertise to support new product designs and developments. Dr. Rakuff received his B.Eng degree from Rudolf Diesel University of Applied Sciences in Augsburg, Germany, in 1998. He was a visiting student at the University of Alabama from 1998 to 1999 and then enrolled as a graduate student at the Center for Precision Engineering at the University of North Carolina at Charlotte, where he received his MS and PhD degrees in mechanical engineering.

Paul Beaudet has 25 years of mechanical engineering experience in the field of manufacturing research and ultraprecision parts fabrication. His experience includes precision manufacturing and machining research applied to nuclear weapons production, establishment of one of the few ultraprecision/diamond turning contract machine shops in the country, and consulting work in precision fabrication for parts requiring sub-millionth-inch (nanometer-level) tolerances. He has extensive experience with optics fabrication, optical and mechanical alignment, diamond turning, laser-guided machine tools, machine tool design and testing, metrology, precision motion, production manufacturing methods for ultraprecision parts, and machining of toxic metals. He has had the opportunity to support critical design review boards for satellite component fabrication for NASA, Lawrence Livermore National Laboratory, and the U.S. Air Force.